arXiv:1611.01097v1 [hep-ph] 3 Nov 2016

Probing Majorana Neutrino Textures at DUNE

Kalpana Bora*

Department of Physics, Gauhati University, Guwahati, Assam 781014, India

Debasish Borah†

Department of Physics, Indian Institute of Technology Guwahati, Assam 781039, India

Debajyoti Dutta‡

Harish-Chandra Research Institute, Chhatnag Road, Jhunsi, Allahabad 211019, India and

Homi Bhabha National Institute, Training School Complex, Anushaktinagar, Mumbai - 400094, India

Abstract

We study the possibility of probing different texture zero neutrino mass matrices at long baseline neutrino experiment DUNE. Assuming a diagonal charged lepton basis and Majorana nature of light neutrinos, we first classify the possible light neutrino mass matrices with one and two texture zeros and then numerically evaluate the parameter space in terms of atmospheric mixing angle θ_{23} and Dirac CP phase $\delta_{\rm CP}$ which satisfies the texture zero conditions. We then feed these parameter values into the numerical analysis in order to study the sensitivity of DUNE experiment to them. We find that the DUNE will be able to exclude some of these texture zero mass matrices which restrict the $(\theta_{23} - \delta_{\rm CP})$ to a very specific range of values.

PACS numbers: 14.60.Pq, 11.10.Gh, 11.10.Hi

* kalpana@gu.ac.in

† dborah@iitg.ernet.in

‡ debajyotidutta@hri.res.in

I. INTRODUCTION

Since the discovery of the Higgs boson in 2012, the large hadron collider (LHC) experiment has been confirming the validity of the standard model (SM) of particle physics again and again without any convincing signature of new physics beyond the standard model (BSM) till date. In spite of such null results, there are plenty of reasons: both theoretical and observational, which undoubtedly suggest the presence of BSM physics. Observation of tiny but non-zero neutrino masses and large leptonic mixing by neutrino oscillation experiments [1–7] is one such reason that has led to a large number of BSM proposals in the last few decades. The current status of neutrino oscillation experiments can be summarised in terms of 3σ global fit values of neutrino parameters shown in table I.

Parameters	NH [8]	IH [8]	NH [9]	IH [9]
$\frac{\Delta m^2_{21}}{10^{-5}\text{eV}^2}$	$7.02 - 8.09(7.50)$	$7.02 - 8.09(7.50)$	$7.11 - 8.18(7.60)$	$7.11 - 8.18(7.60)$
$\frac{\lvert\Delta m^2_{31}\rvert}{10^{-3}\text{eV}^2}$	$2.317 - 2.607(2.457)$	$2.307 - 2.590(2.449)$	$2.30 - 2.65(2.48)$	$2.20 - 2.54(2.38)$
$\frac{\sin^2\theta_{12}}{10^{-1}}$	$2.70 - 3.44(3.04)$	$2.70 - 3.44(3.04)$	$2.78 - 3.75(3.23)$	$2.78 - 3.75(3.23)$
$\frac{\sin^2\theta_{23}}{10^{-1}}$	$3.82 - 6.43\ (4.52)$	$3.89 - 6.44(5.79)$	$3.93 - 6.43(5.67)$	$4.03 - 6.40(5.73)$
$\frac{\sin^2\theta_{13}}{10^{-2}}$	$1.86 - 2.50(2.18)$	$1.88 - 2.51(2.19)$	$1.90 - 2.62(2.34)$	$1.93 - 2.65(2.40)$
δ	$0 - 2\pi(1.7\pi)$	$0 - 2\pi(1.41\pi)$	$0 - 2\pi(1.34\pi)$	$0 - 2\pi(1.48\pi)$

TABLE I. Global fit 3σ range and the best fit values (in brackets) of neutrino oscillation parameters [8, 9].

where NH and IH refer to normal and inverted hierarchical neutrino masses respectively. The above data also allow the possibility of quasi-degenerate neutrinos ($m_1 \approx m_2 \approx m_3$). Although the question of the absolute mass scale of neutrinos remain open at oscillation experiments, cosmology and neutrinoless double beta decay ($0\nu\beta\beta$) experiments put upper bound on the lightest neutrino mass. For example, the latest Planck experiment data constrain the sum of absolute neutrino masses as $\sum_i |m_i| < 0.17$ eV [12]. Similarly, constraints from the ongoing ($0\nu\beta\beta$) experiments [14–16] rule out light neutrino masses around 0.1 eV and above. On the other hand, the leptonic Dirac CP phase δ_{CP} remains undetermined as of now, though a recent hint towards $\delta_{\text{CP}} \approx -\pi/2$ [17] appeared recently from the T2K

collaboration. If neutrinos are Majorana fermions, then two Majorana CP phases come into the picture which however, do not affect neutrino oscillation probabilities, but can be probed at $(0\nu\beta\beta)$ experiments.

In the three flavor neutrino oscillation scenario, the oscillations are driven by the two mass square differences Δm^2_{21} and Δm^2_{31}. Out of the three mixing angles, θ_{12}, θ_{13} and θ_{23} governing the oscillation amplitudes, θ_{12} and θ_{13} are very precisely measured. Although the atmospheric mixing angle θ_{23} was measured in 1998 at Super-Kamiokande atmospheric neutrino experiment, yet it is not confirmed if $\theta_{23} = 45^0$ i.e. maximal or not. If not, then it lies either in the higher octant (HO) ($\theta_{23} > 45^0$) or in the lower octant (LO) ($\theta_{23} < 45^0$). The preliminary results from T2K experiment [3, 17] prefers near maximal mixing [18] while MINOS [7, 19] and Super-Kamiokande (SK) disfavor maximal mixing [20]. All the global analyses are inconsistent with maximal θ_{23} at less than 1σ [8, 9, 21]. Recent NOνA data exclude the maximal mixing scenario at 2.5σ C.L. [22] favoring the case of two degenerate solutions. So in the present scenario, we have to wait for the long baseline accelerator experiments to resolve this ambiguity as well as to measure θ_{23} precisely. The capability of DUNE [23, 24], NOνA [25, 26], T2K etc to resolve octant ambiguity has been studied in [27–29]. Octant sensitivity at DUNE in conjunction with reactor experiments is studied in [30, 31]. These long baseline (LBL) accelerator experiments are sensitive to both $\nu_\mu \to \nu_e$ (appearance) and $\nu_\mu \to \nu_\mu$ (disappearance) and synergy between them can enhance the octant sensitivity [32, 33]. On the other hand, any terrestrial baseline of several hundred kilometers is sensitive to matter effect. So these LBL experiments, being sensitive to matter effect can discriminate between the two hierarchies [23, 34].

After the precise measurement of θ_{13}, now the whole neutrino community is focusing on the leptonic CP phase $\delta_{\rm CP}$, which is the only unknown parameter in the three flavor oscillation framework. Although in the quark sector, CP violation is observed and can be explained due to complex Yukawa couplings or complex Higgs field vacuum expectation values [35, 36], it is yet to be discovered in the leptonic sector with some significant degree of precision. The LBL accelerator experiments which are sensitive to $\nu_\mu \to \nu_e$ channel can probe CP violation in the leptonice sector [23]. From this point of view, the DUNE (Deep Underground Neutrino Experiment) at Fermilab, U.S. is the best candidate which will start taking data from 2025. In the literature, recent studies related to CP violation discovery potential of DUNE as well as other superbeam experiments can be found [37–41].

Before the neutrino oscillation experiments completely remove the existing ambiguities in neutrino parameters like the octant of θ_{23}, Dirac CP phase as well as mass hierarchy at ongoing and near future experiments, it is important to study the predictions for these neutrino observables within different BSM frameworks. Depending on the predictions for such neutrino observables, one can discriminate between different BSM scenarios at the oscillation experiments. However, generic BSM frameworks come with several free parameters, making it difficult to have a robust prediction for a particular neutrino parameter. Reducing the number of free parameters can therefore lead to robust testable predictions of neutrino observables. Such reduction of free parameters can be possible within the framework of flavour symmetry models where the additional discrete or continuous symmetries either relate two or more terms or forbid some terms in the mass matrix. One such possibility arises within the context of texture zeros in leptonic mass matrices. For a complete survey of such texture zeros in lepton mass matrices, please refer to [42]. Different possible flavour symmetric interpretation for the origin of such texture zero mass matrices can be found in[43–52] within the framework of different seesaw models. Such texture zero mass matrices in general, have specific predictions for neutrino oscillation parameters, the consequences of which can be studied from cosmology as well as oscillation experiments point of view. In the light of neutrino oscillation experiment data, one-zero and two-zero texture mass matrices were studied in [53–56] and [52, 57–69] respectively. These texture zero mass matrices were also studied from leptogenesis point of view in [70–76].

In this work, we do a phenomenological study of one-zero and two-zero texture mass matrices at DUNE. The main motive of this work is to find if any of these textures can be ruled out, focusing on the sensitivity of neutrino oscillation experiments like DUNE to the values of $\theta_{23}, \delta_{\rm CP}$ predicted by a particular texture zero mass matrix. We first numerically determine the values of $\theta_{23}, \delta_{\rm CP}$ which satisfy a a particular texture zero condition and then use them in GLoBES software [77, 78] to determine the corresponding experimental sensitivity. We show that these textures can be excluded for some combinations of θ_{23} and $\delta_{\rm CP}$ at DUNE. The results presented here reveal that the two-zero textures can give more precise measurements compared to one-zero textures. And also, if NH is the true hierarchy then B4 texture with two zeros can give the most precise measurement in $\theta_{23} - \delta_{\rm CP}$ parameter space.

The paper has been organised as follows. In section II, we discuss about the theory of different textures. A brief discussion on DUNE is presented in section III. Section IV contains the details of our numerical analysis while in section V we present our results and discussions. Concluding remarks are given in section VI.

II. TEXTURE ZEROS IN MAJORANA NEUTRINO MASS MATRIX

If light neutrinos are of Majorana nature, the 3×3 mass matrix M_ν is complex symmetric having six independent complex parameters. In such a scenario, the total number of structurally different Majorana neutrino mass matrices with k texture zeros is given by

$$^6C_k = \frac{6!}{k!(6-k)!} \tag{1}$$

A symmetric mass matrix with more than three texture zeros is not compatible with the observed leptonic mixing and masses. The Pontecorvo-Maki-Nakagawa-Sakata (PMNS) leptonic mixing matrix is related to the diagonalising matrices of charged lepton and neutrino mass matrices as

$$U_{\rm PMNS} = U_l^\dagger U_\nu \tag{2}$$

In the diagonal charged lepton basis, $U_{\rm PMNS}$ is same as the diagonalising matrix U_ν of the neutrino mass matrix M_ν. In this basis, it was shown [79] that a symmetric Majorana neutrino mass matrix with 3 texture zeros is not compatible with neutrino oscillation data. This leaves us with the possible one-zero and two-zero texture mass matrices. Going by the counting formula mentioned above (1), we can have six possible one-zero texture and fifteen possible two-zero texture mass matrices. The one-zero texture mass matrices can be written as

$$G_1 : \begin{pmatrix} 0 & \times & \times \\ \times & \times & \times \\ \times & \times & \times \end{pmatrix}, G_2 : \begin{pmatrix} \times & 0 & \times \\ 0 & \times & \times \\ \times & \times & \times \end{pmatrix}, G_3 : \begin{pmatrix} \times & \times & 0 \\ \times & \times & \times \\ 0 & \times & \times \end{pmatrix}, G_4 : \begin{pmatrix} \times & \times & \times \\ \times & 0 & \times \\ \times & \times & \times \end{pmatrix},$$

$$G_5 : \begin{pmatrix} \times & \times & \times \\ \times & \times & 0 \\ \times & 0 & \times \end{pmatrix}, G_6 : \begin{pmatrix} \times & \times & \times \\ \times & \times & \times \\ \times & \times & 0 \end{pmatrix} \tag{3}$$

Where the crosses "$\times$" denote non-zero arbitrary elements of M_ν. Similarly, the two-zero texture matrices, classified into six categories (following the notations of [65]) are given by

$$A_1 : \begin{pmatrix} 0 & 0 & \times \\ 0 & \times & \times \\ \times & \times & \times \end{pmatrix}, A_2 : \begin{pmatrix} 0 & \times & 0 \\ \times & \times & \times \\ 0 & \times & \times \end{pmatrix}; \tag{4}$$

$$B_1 : \begin{pmatrix} \times & \times & 0 \\ \times & 0 & \times \\ 0 & \times & \times \end{pmatrix}, B_2 : \begin{pmatrix} \times & 0 & \times \\ 0 & \times & \times \\ \times & \times & 0 \end{pmatrix}, B_3 : \begin{pmatrix} \times & 0 & \times \\ 0 & 0 & \times \\ \times & \times & \times \end{pmatrix}, B_4 : \begin{pmatrix} \times & \times & 0 \\ \times & \times & \times \\ 0 & \times & 0 \end{pmatrix}; \tag{5}$$

$$C : \begin{pmatrix} \times & \times & \times \\ \times & 0 & \times \\ \times & \times & 0 \end{pmatrix}; \tag{6}$$

$$D_1 : \begin{pmatrix} \times & \times & \times \\ \times & 0 & 0 \\ \times & 0 & \times \end{pmatrix}, D_2 : \begin{pmatrix} \times & \times & \times \\ \times & \times & 0 \\ \times & 0 & 0 \end{pmatrix}; \tag{7}$$

$$E_1 : \begin{pmatrix} 0 & \times & \times \\ \times & 0 & \times \\ \times & \times & \times \end{pmatrix}, E_2 : \begin{pmatrix} 0 & \times & \times \\ \times & \times & \times \\ \times & \times & 0 \end{pmatrix}, E_3 : \begin{pmatrix} 0 & \times & \times \\ \times & \times & 0 \\ \times & 0 & \times \end{pmatrix}; \tag{8}$$

$$F_1 : \begin{pmatrix} \times & 0 & 0 \\ 0 & \times & \times \\ 0 & \times & \times \end{pmatrix}, F_2 : \begin{pmatrix} \times & 0 & \times \\ 0 & \times & 0 \\ \times & 0 & \times \end{pmatrix}, F_3 : \begin{pmatrix} \times & \times & 0 \\ \times & \times & 0 \\ 0 & 0 & \times \end{pmatrix}, \tag{9}$$

Where the crosses "$\times$" imply non-zero arbitrary elements of M_ν. The latest neutrino oscillation data on mixing angles. mass squared differences and cosmology data on sum of absolute neutrino masses allow only six different two-zero textures $A_{1,2}$ and $B_{1,2,3,4}$ as shown by [65, 67].

III. DUNE AT A GLANCE

The Deep Underground Neutrino Experiment (DUNE) is a future accelerator experiment to be online in ~ 2025. The experimental specifications are almost similar to earlier planned

LBNE [23]. DUNE is designed in such a way that it can answer all the three most important questions in the neutrino sector - mass hierarchy, octant of θ_{23} and existence of CP violation in the leptonic sector. The $\nu_\mu(\bar{\nu}_\mu)$ super-beam from Fermilab will be detected by a 35-40 kt Liquid Argon (LAr) far detector at a distance of 1300 km in the Homestake mine, South Dakota. The experiment plans to run for 10 years both in anti-neutrino (5 years) and neutrino (5 years) mode. A 1.2 MW - 120 GeV proton beam will deliver 10^{21} protons-on-target (POT) per year which corresponds to a total exposure of 35×10^{22} kt-POT-yr.

All other details, such as signal and background channels, signal efficiencies are taken from [23, 24] and tabulated in Table II and Table III.

Experiment	Signal	Signal norm error	Background norm error	Calibration error	
				Signal	Background
DUNE	ν_e	5%	10%	5%	5%
	ν_μ	5%	10%	5%	5%

TABLE II. Systematics uncertainties for DUNE

Experiment	Signal	Signal Efficiencies	Energy Resolutions	Runtime (yrs) $\nu + \bar{\nu}$	Detector Mass (Type)
DUNE	ν_e^{CC}	80%	$0.15/\sqrt{E}$	5 + 5	35 kton (LArTPC)
	ν_μ^{CC}	85%	$0.20/\sqrt{E}$		

TABLE III. Simulation details like signal efficiencies, energy resolutions, total exposures and detector mass for DUNE

IV. NUMERICAL ANALYSIS

In the diagonal charged lepton basis, $U_{\rm PMNS}$ is same as the diagonalizing matrix U_ν which can be parametrized as

$$U_{\rm PMNS} = \begin{pmatrix} c_{12}c_{13} & s_{12}c_{13} & s_{13}e^{-i\delta_{\rm CP}} \\ -s_{12}c_{23} - c_{12}s_{23}s_{13}e^{i\delta_{\rm CP}} & c_{12}c_{23} - s_{12}s_{23}s_{13}e^{i\delta_{\rm CP}} & s_{23}c_{13} \\ s_{12}s_{23} - c_{12}c_{23}s_{13}e^{i\delta_{\rm CP}} & -c_{12}s_{23} - s_{12}c_{23}s_{13}e^{i\delta_{\rm CP}} & c_{23}c_{13} \end{pmatrix} {\rm diag}(1, e^{i\alpha}, e^{i(\beta+\delta_{\rm CP})}) \tag{10}$$

where $c_{ij} = \cos\theta_{ij}$, $s_{ij} = \sin\theta_{ij}$. $\delta_{\rm CP}$ is the Dirac CP phase and α, β are the Majorana phases. Using the parametric form of PMNS matrix shown in (10), the Majorana neutrino mass matrix M_ν can be found as

$$M_\nu = U_{\rm PMNS} M_\nu^{\rm diag} U_{\rm PMNS}^T \tag{11}$$

where

$$M_\nu^{\rm diag} = \begin{pmatrix} m_1 & 0 & 0 \\ 0 & m_2 & 0 \\ 0 & 0 & m_3 \end{pmatrix}, \tag{12}$$

where m_1, m_2 and m_3 are the three neutrino mass eigenvalues. For the case of normal hierarchy, the three neutrino mass eigenvalues can be written as

$$M_\nu^{\rm diag} = {\rm diag}(m_1, \sqrt{m_1^2 + \Delta m_{21}^2}, \sqrt{m_1^2 + \Delta m_{31}^2})$$

while for the case of inverted hierarchy, it can be written as

$$M_\nu^{\rm diag} = {\rm diag}(\sqrt{m_3^2 + \Delta m_{23}^2 - \Delta m_{21}^2}, \sqrt{m_3^2 + \Delta m_{23}^2}, m_3)$$

The analytical expressions of the elements of this mass matrix are given in Appendix A.

From the parametrisation of light neutrino mass matrix, it can be seen that there are nine parameters: three masses, three angles and three phases. Out of these five parameters namely, two mass squared differences and three mixing angles are measured in several experiments and their best fit values along with 3σ ranges are shown in table I. It is worth noting that there still remains some ambiguity in determining the octant of θ_{23}. Apart from this, the three CP phases and the lightest neutrino mass and hence the type of mass hierarchy are yet to be determined experimentally. Due to the predictive nature of texture

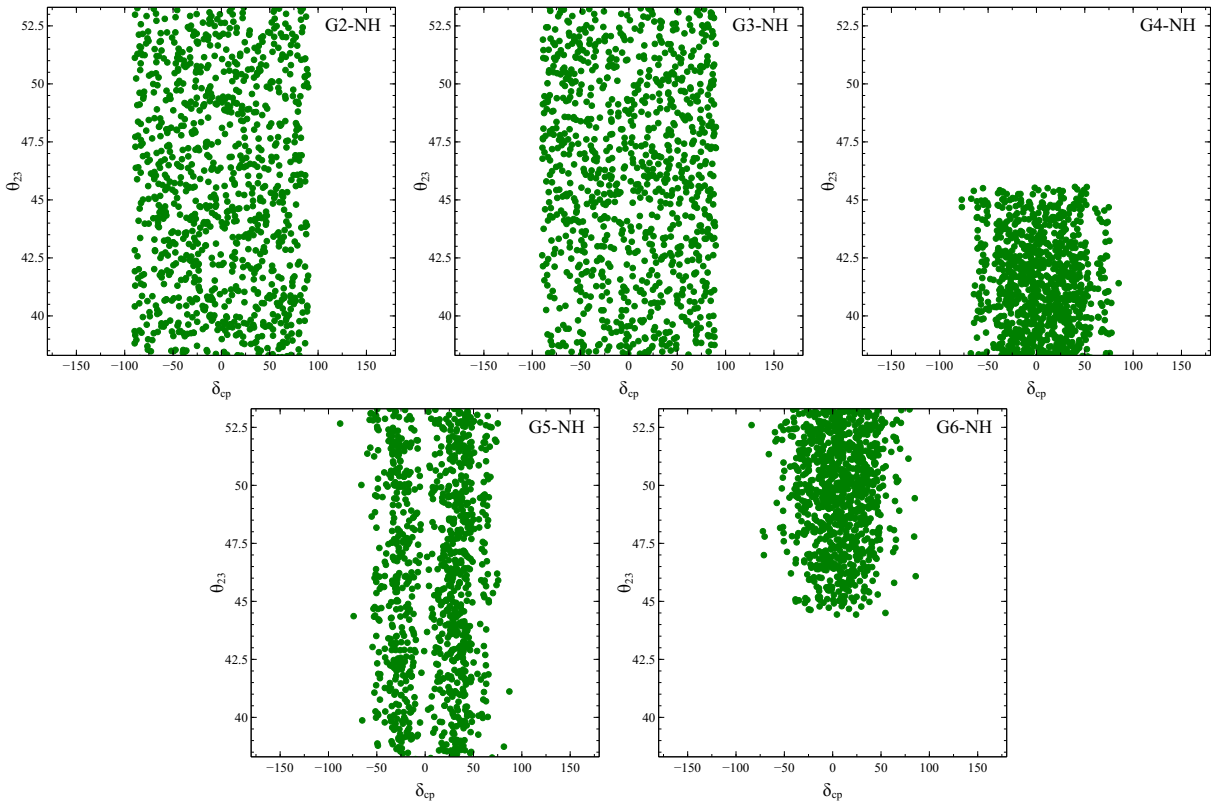

FIG. 1. Neutrino parameters corresponding to one-zero textures for true NH

zero mass matrices and upcoming neutrino experiment like DUNE having the potential to settle the issue of θ_{23} octant, Dirac CP phase $\delta_{\rm CP}$ as well as mass hierarchy we first numerically evaluate the neutrino parameters for a particular texture zero mass matrix using the best fit values of two angles θ_{12}, θ_{13}, two mass squared differences from the global fit reference [8]. For each possible one-zero texture mass matrix, we have one complex or two real equations which can be solved numerically to evaluate $\theta_{23}, \delta_{\rm CP}$. Since the M_{ee} element of the light neutrino mass matrix does not depend upon $\delta_{\rm CP}$ as seen from the analytical expressions given in appendix A, we do not take the one-zero texture denoted as G_1 into account. For the other five one-zero texture mass matrices, we solve the two real equations corresponding to the texture zero condition and determine the parameter space in terms of $\theta_{23}, \delta_{\rm CP}$. The corresponding regions of parameter space are shown in figure 1, 2 for NH and IH respectively. Similarly, we numerically solve the two complex or four real equations for the two-zero texture mass matrices $A_{1,2}, B_{1,2,3,4}$ and extract the resulting parameter space.

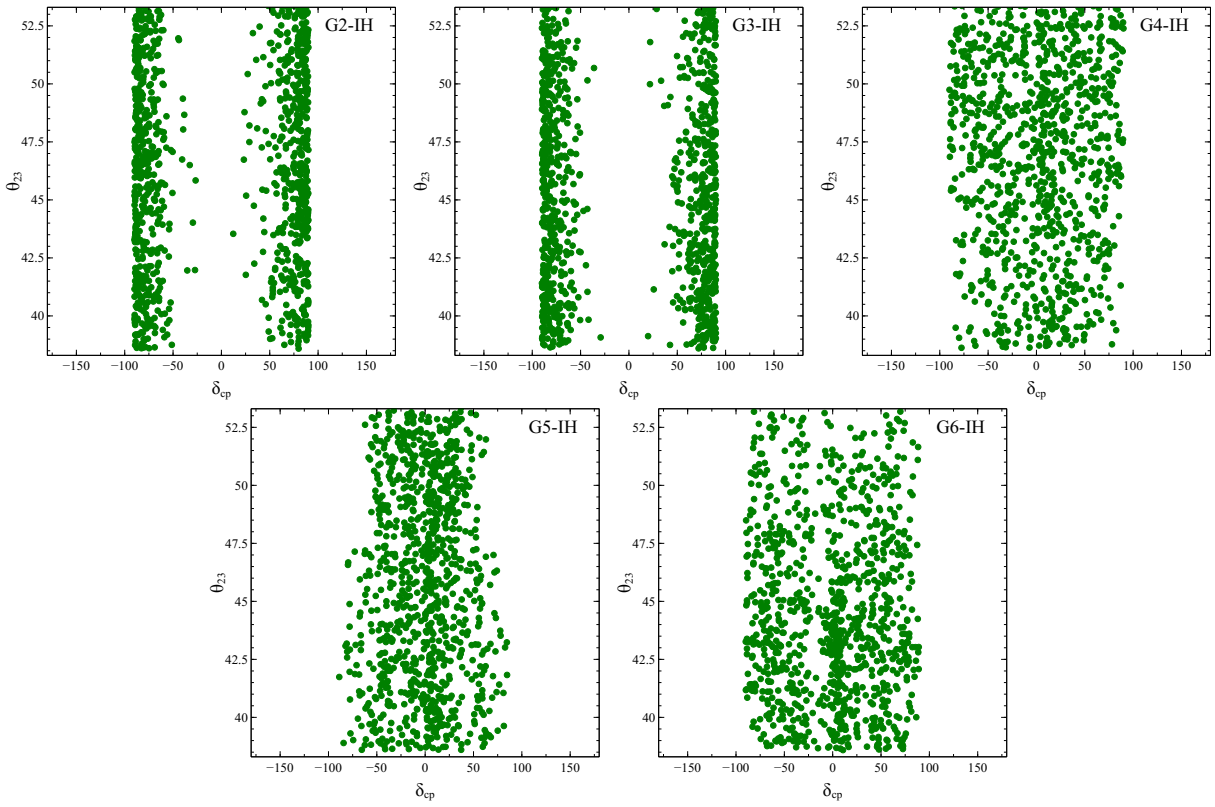

FIG. 2. Neutrino parameters corresponding to one-zero textures for IH

They are shown in figure 3, 4 for NH and IH respectively. We find that the use of the latest best fit values of solar and reactor mixing angles as well as the two mass squared differences allow only three two-zero textures with NH and four two-zero textures with IH. This is in contrast with the six allowed two-zero texture matrices shown in earlier works [65, 67].

After numerically evaluating the neutrino parameters $\theta_{23}, \delta_{\rm CP}$ for the texture zero mass matrices, we move on to studying the sensitivity of long baseline experiment DUNE to such parameter values. As stated in introduction, in this work we aim to study the sensitivity of different neutrino mass textures at DUNE (i.e. if DUNE can rule out the existence of a given texture). For this, we have used the present best fit values of the standard 3ν oscillation parameters as the 'true values' or 'data'. The best fit values of the oscillation parameters are taken from [8]. To test the sensitivity of a particular texture, the values of the neutrino oscillation parameters from the texture zero conditions are used as 'fit' values and then χ^2

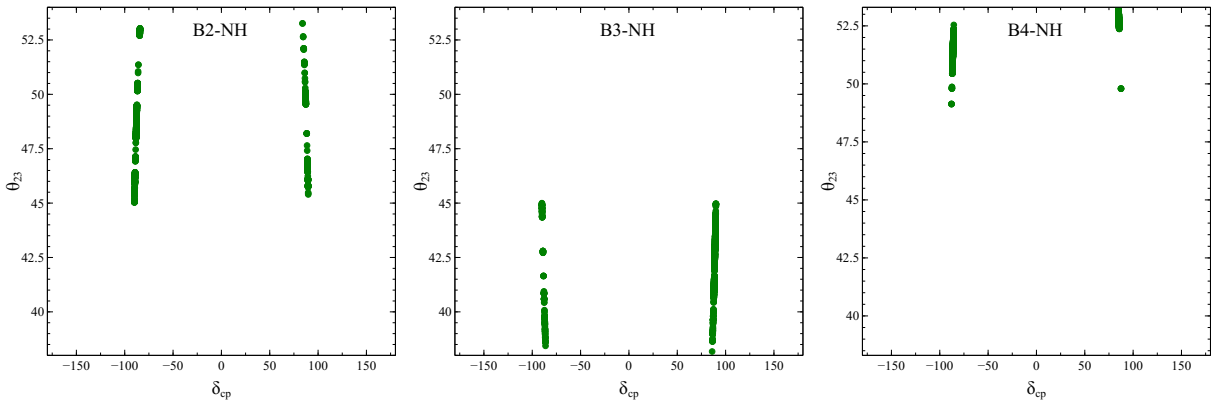

FIG. 3. Neutrino parameters corresponding to two-zero textures for NH

is calculated between 'data' and 'fit'. We define the χ^2 as:

$$\chi^2 = \sum_{i=1}^{bins} \sum_{j}^{2} \frac{[N_{true}^{i,j} - N_{test}^{i,j}]^2}{N_{true}^{i,j}}, \tag{13}$$

where $N_{true}^{i,j}$ and $N_{test}^{i,j}$ are the event rates that correspond to 'data' and 'fit' in the i^{th} bin. $j = 1$ is for neutrinos and $j = 2$ for anti-neutrinos. We have considered 39 bins for DUNE each of width 250 MeV in the energy range 0.5 to 10 GeV.

We show our sensitivity results in terms of $\delta_{\rm CP}$ as it is the least known parameter in the three flavor framework. Since, there is still some tension in the measurements of θ_{23}, we have varied it in its 3σ allowed range [8] in 'data' to show the maximum sensitivity. For an assumed true hierarchy, we have also shown the sensitivity for three specific cases: maximal θ_{23} ($\theta_{23} = 45^0$), θ_{23} in the lower octant ($\theta_{23} < 45^0$) and θ_{23} in the higher octant ($\theta_{23} > 45^0$). In the LO, we consider the present best fit value [8] of θ_{23} as the true value and hence $(90^0 - \theta_{23})$ is the true θ_{23} in the HO. For each set of true values, we have varied θ_{23} and $\delta_{\rm CP}$ (which are different for each texture) in 'fit', and then calculate the χ^2. Then for each true $\delta_{\rm CP}$ we calculate the minimised χ^2 (i.e. $\chi^2_{\rm min}$). We also show the minimum and maximum of $\chi^2_{\rm min}$ which is obtained corresponding to the variation of true θ_{23} in its allowed 3σ range for each true $\delta_{\rm CP}$.

We have also shown the exclusion plots in the θ_{23}(true) $-$ $\delta_{\rm CP}$(true) parameter space. Here, the contours are defined by $\chi^2 > 4$ (9) which corresponds to 2σ (3σ) C.L.. So for a given texture and for a given set of true θ_{23} and $\delta_{\rm CP}$, if the test θ_{23} and $\delta_{\rm CP}$ gives $\chi^2 > 4(9)$,

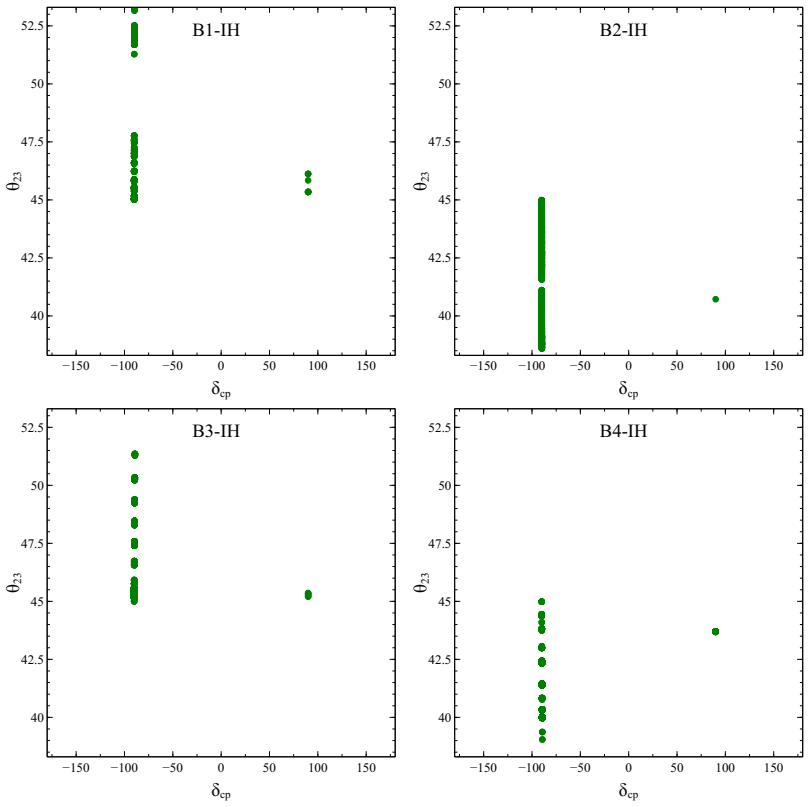

FIG. 4. Neutrino parameters corresponding to two-zero textures for IH

then we can say that the texture can be excluded at 2σ (3σ) C.L.. Otherwise, for $\chi^2 < 4(9)$, the texture can not be excluded at 2σ (3σ) C.L..

V. RESULTS AND DISCUSSIONS

In this section, we have presented our results. We have tested two textures at DUNE - one zero and two zero. Each set of textures are tested for both the hierarchies.

In fig. 7, the upper panel (UP) shows the sensitivity of G2, G3, G4, G5 and G6 textures (generated assuming true NH) while the lower panel (LP) shows the allowed/exclusion regions at DUNE. Here, the solid red (blue) line corresponds to true $\theta_{23} = 42.3$ (47.7) i.e. θ_{23} in the LO (HO) and the green line corresponds to maximal θ_{23} i.e. $\theta_{23} = 45^0$. For each true $\delta_{\rm CP}$, we calculate the minimum and maximum of $\chi^2_{\rm min}$ corresponding to variation of θ_{23} in its 3σ allowed range. From the plots corresponding to three different values of θ_{23} we can

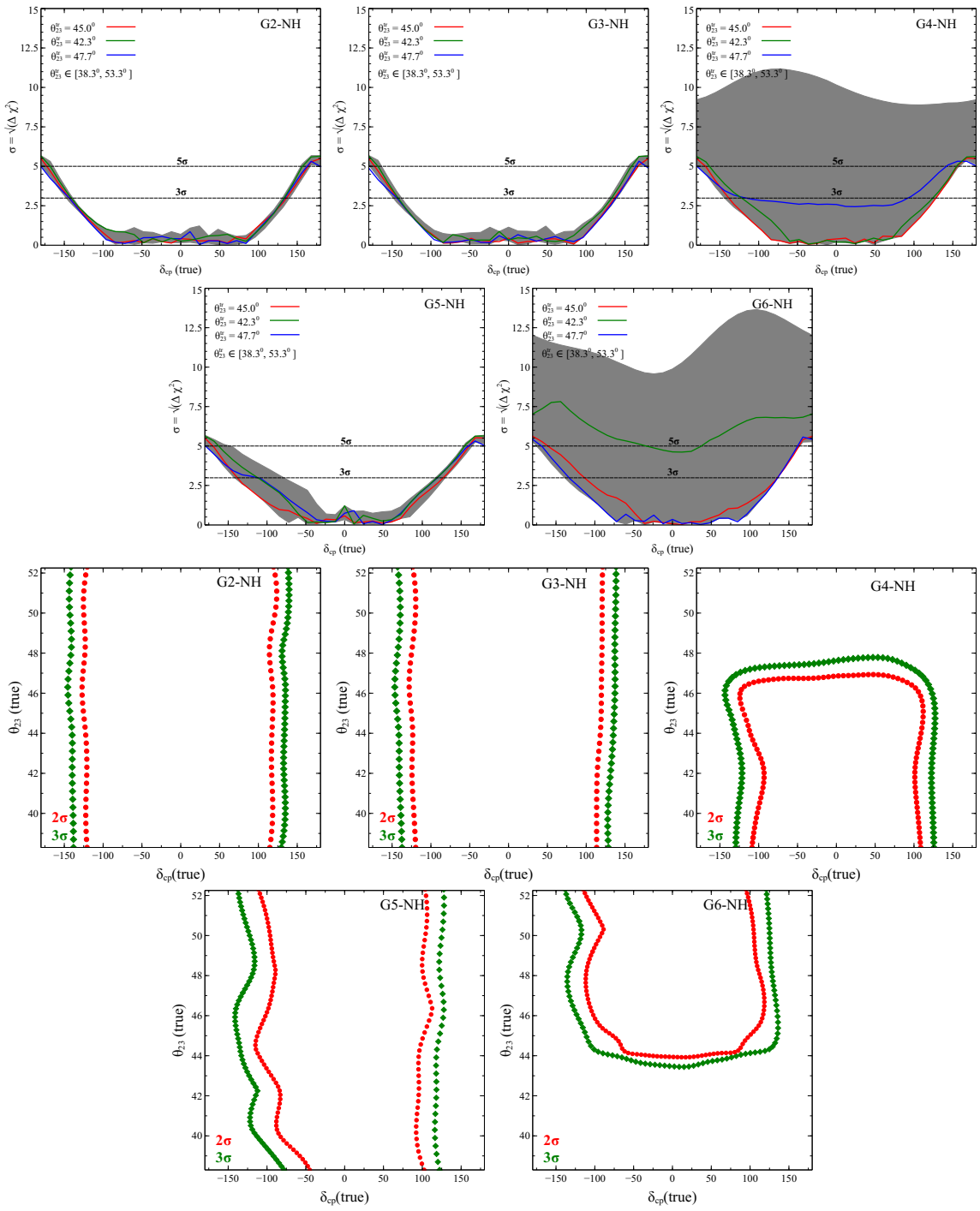

FIG. 5. The sensitivity of different one-zero textures at DUNE assuming NH as the true hierarchy. In the upper panel, the grey band represents the full variation of θ_{23} in its 3σ allowed range. Green, blue and the red plots corresponds to three different choice of θ_{23} i.e. green plot is for the best fit value of θ_{23} in the LO while the blue plot is for θ_{23} in the HO. The red plot is for maximal θ_{23}. In the contour plot, green (red) dotted line represents the 3σ (2σ) contour at 1 d.o.f..

draw the following conclusions:

- **G2-NH, G3-NH** Both G2 and G3 show almost similar behaviours. It is seen that the χ^2 behaviour is almost same for all values of θ_{23} and the whole range of $\delta_{\rm CP}$ is allowed at 5σ C.L. except a small fraction around $\pm\pi$. On the other hand, the 3σ allowed range for $\delta_{\rm CP}$ is from -150^0 to 137^0 (approx) which can also be confirmed from the contour plots in the LP.

- **G4-NH** DUNE can not exclude this texture at 5σ C.L. for the three specific choice of θ_{23} for $\delta_{\rm CP} < 150^0$ and $\delta_{\rm CP} > -160^0$ (approx). If HO (LO) is the true octant, then at 3σ C.L., DUNE can exclude G4 for all $\delta_{\rm CP} < -125^0$ ($\delta_{\rm CP} < -125^0$) and $\delta_{\rm CP} > 100^0$ ($\delta_{\rm CP} > 125^0$). Similarly, if $\theta_{23} = 45^0$, for all $\delta_{\rm CP} < -137^0$ and $\delta_{\rm CP} > 125^0$, DUNE excludes G4 at 3σ.

- **G5-NH** Behaviour of G5 is somewhat like G2 and G3 at 5σ C.L.. As seen from the contour plot corresponding to G5-NH, the region excluded at 3σ is slightly higher compared to G2 and G3 and hence there is slight improvement in predictability of this texture at DUNE.

- **G6-NH** If LO is the true octant then DUNE can exclude G6 at 5σ for all $\delta_{\rm CP} < -37^0$ and $\delta_{\rm CP} > 37^0$. But for the other two choices of θ_{23}, 5σ exclusion of G6 is only possible around $\delta_{\rm CP} = \pm\pi$.

- From the contour plots, we observe that, more than 70% of the $\theta_{23} - \delta_{\rm CP}$ parameter space is allowed in case of G2, G3 and G5 while the allowed region is much constrained in case of G4 and G6. So, G4 and G6 are more predictive. In case of G4, most of the space in the HO is excluded while in G6, the excluded region is in the LO.

In fig.6, we show the sensitivity and exclusion plots for G2, G3, G4, G5 and G6 textures assuming true IH. We draw the following observations from fig.6:

- **G2-IH, G3-IH** The sensitivity plots for these two textures look very similar for the three specific choice of θ_{23}. None of them can be excluded at 5σ for these three choice of θ_{23} and for all $\delta_{\rm CP}$ except $\delta_{\rm CP} > 150^0$. At 3σ C.L., the CP conserving scenarios are excluded for the best fit value of θ_{23} in both the octant. But for maximal θ_{23}, Only

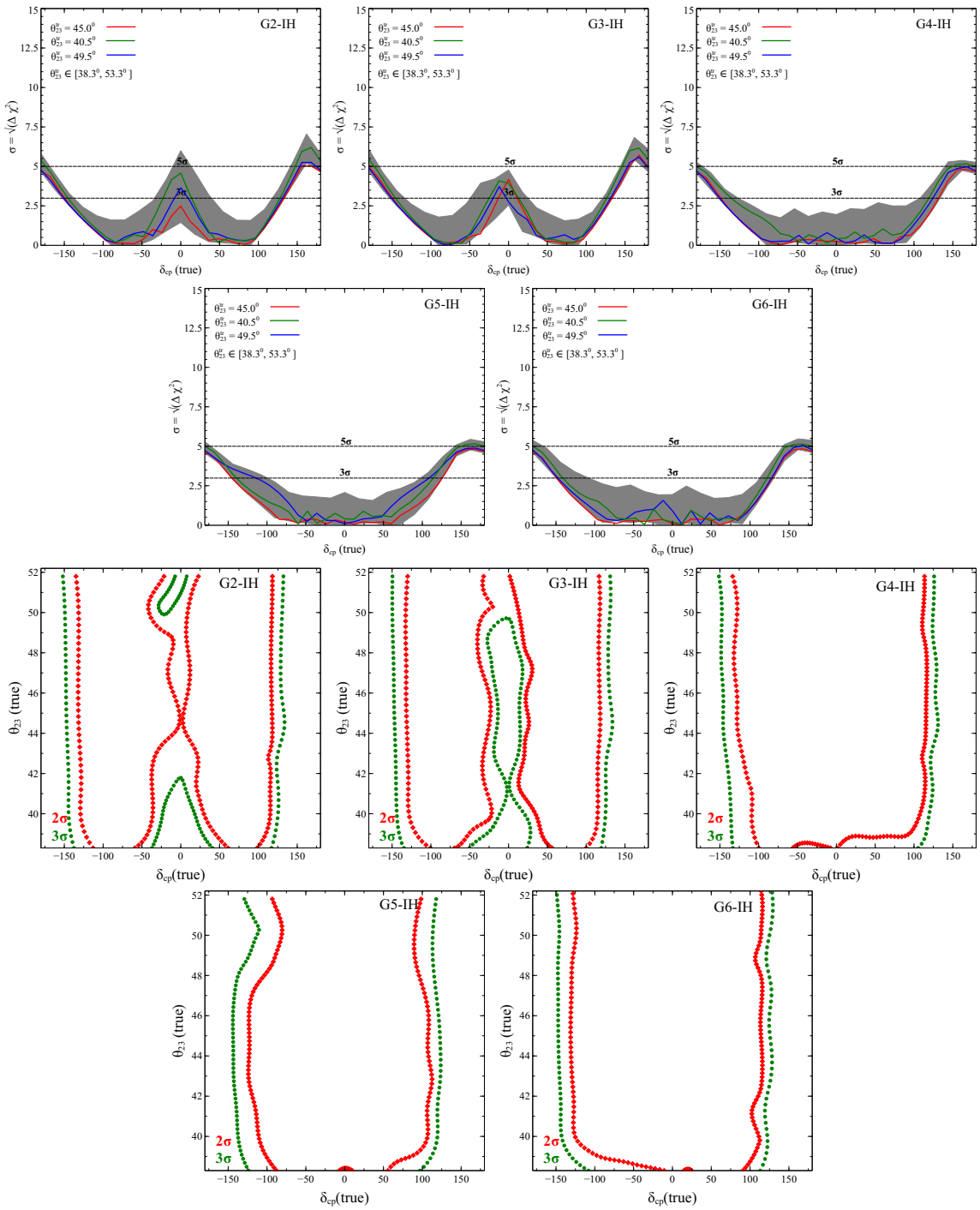

FIG. 6. The sensitivity of different one-zero textures at DUNE assuming IH as the true hierarchy. In the upper panel, the grey band represents the full variation of θ_{23} in its 3σ allowed range. Green, blue and the red plots corresponds to three different choice of θ_{23} i.e. green plot is for the best fit value of θ_{23} in the LO while the blue plot is for θ_{23} in the HO. The red plot is for maximal θ_{23}. In the contour plot, green (red) dotted line represents the 3σ (2σ) contour at 1 d.o.f..

G3 can exclude $\delta_{\rm CP} = 0^0$ at 3σ. It can also be verified from the contour plots for G2 and G3.

- **G4-IH, G5-IH, G6-IH** The sensitivity plots corresponding to these three textures are very similar and DUNE can exclude them at 5σ only for $\delta_{\rm CP} > 150^0$ when true θ_{23} is in the LO. It is observed from the contour plots that more than 75% of $\theta_{23} - \delta_{\rm CP}$ parameter space is allowed for these textures in IH mode. For true $\delta_{\rm CP}$ from -150^0 to 125^0, all values of θ_{23} are allowed. Hence these three textures are less predictive than G2 and G3 in IH mode.

In fig. 7, the upper panel (UP) shows the sensitivity of B2, B3 and B4 textures (generated assuming true NH) while the lower panel (LP) shows the allowed/exclusion regions at DUNE. We can draw the following conclusions:

- **B2-NH:** When θ_{23} is in the LO, B2 can be excluded at DUNE for almost all values of $\delta_{\rm CP}$ (except the cp conserving values of $\delta_{\rm CP}$) at 5σ C.L.. On the other hand, when θ_{23} is maximal and it lies in the HO, at 5σ C.L., almost all values of $\delta_{\rm CP}$ are allowed and at 3σ, $-150^0 < \delta_{\rm CP} < -40^0$ and $40^0 < \delta_{\rm CP} < 130^0$ are allowed. This can also be seen in the LP figures where the region inside the contours are the allowed region.

- **B3-NH:** When θ_{23} lies in the LO, $\delta_{\rm CP}$ in the range $-160^0 < \delta_{\rm CP} < -10^0$ and $20^0 < \delta_{\rm CP} < 155^0$ are the allowed at 5σ C.L. while at 3σ, the allowed range are $-130^0 < \delta_{\rm CP} < -45^0$ and $45^0 < \delta_{\rm CP} < 135^0$. When θ_{23} is maximal, B3 is allowed for almost all values of $\delta_{\rm CP}$ at 5σ C.L. except a small region near the CP conserving values and at 3σ C.L., the texture is allowed almost for 50% of true $\delta_{\rm CP}$. But, when θ_{23} is in the HO, DUNE can exclude B3 at 3σ C.L. except for a small fraction of $\delta_{\rm CP}$ in the range $-137^0 < \delta_{\rm CP} < -75^0$.

- **B4-NH:** In this case, the texture can be excluded at 3σ C.L. for all the three specific values of θ_{23}. When θ_{23} is maximal or in the LO, B4 can be excluded at 5σ irrespective of any true $\delta_{\rm CP}$. But at 5σ, B4 is allowed at DUNE when $\delta_{\rm CP}$ is in the range $-150^0 < \delta_{\rm CP} < -37^0$ and θ_{23} is the HO.

- In the LP, the contours are drawn at 2σ (red circle) and 3σ (green diamond) C.L. for the three textures: B2, B3 and B4 in NH mode. The region within the red line (green

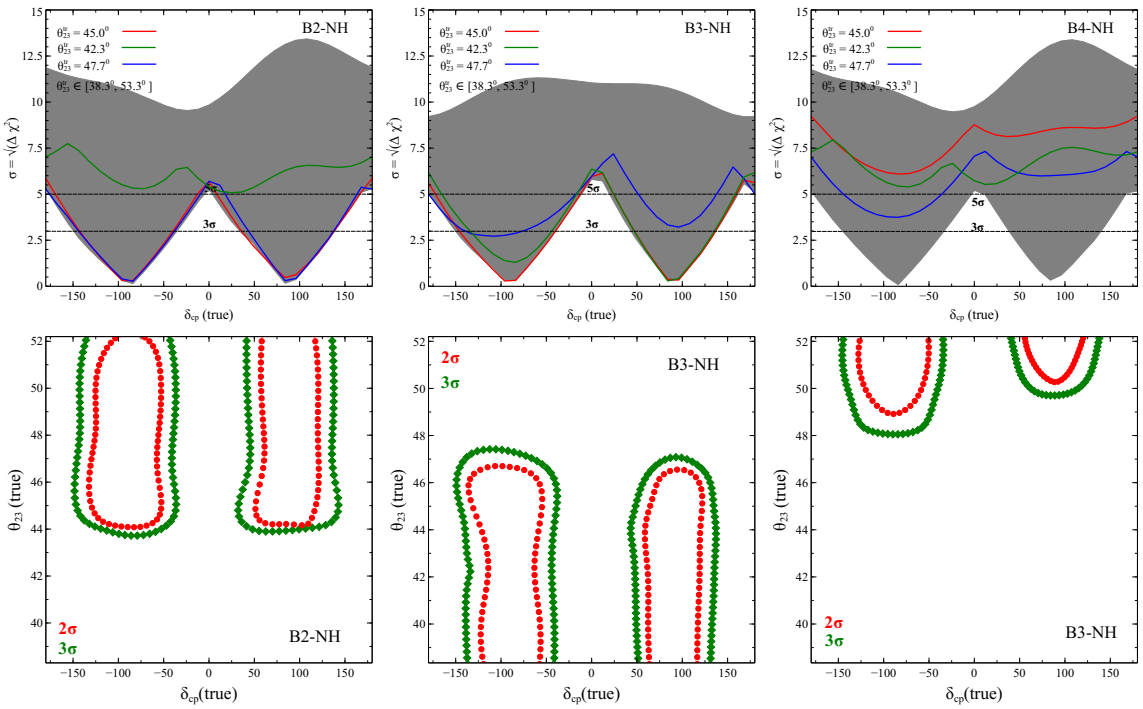

FIG. 7. The sensitivity of different two-zero textures at DUNE assuming NH as the true hierarchy. In the upper panel, the grey band represents the full variation of θ_{23} in its 3σ allowed range. Green, blue and the red plots corresponds to three different choice of θ_{23} i.e. green plot is for the best fit value of θ_{23} in the LO while the blue plot is for θ_{23} in the HO. The red plot is for maximal θ_{23}. In the contour plot, green (red) dotted line represents the 3σ (2σ) contour at 1 d.o.f..

line) is defined by $\chi^2 < 4$ (9). The region in between the red and green line is such that $4 < \chi^2 < 9$. So for all the points inside the red (green) line, these textures can not be excluded at 2σ (3σ), i.e. the allowed region in $\theta_{23} - \delta_{\rm CP}$ true parameter space. But all the regions outside the green (red) contour is the excluded region for that particular texture at 3σ (2σ). The regions allowed in case of B2 and B4 are almost equal but lie in the opposite octant. While in case of B4, the most of the parameter space is excluded and the allowed region in this case is much smaller than B2 and B3. Hence B4 is more predictive than B2 and B3 and it prefer HO as the true octant.

In fig.8, we have shown our results for B1, B2, B3 and B4 textures assuming IH as the true hierarchy. In the two upper panels, we have shown the sensitivity plots. Following

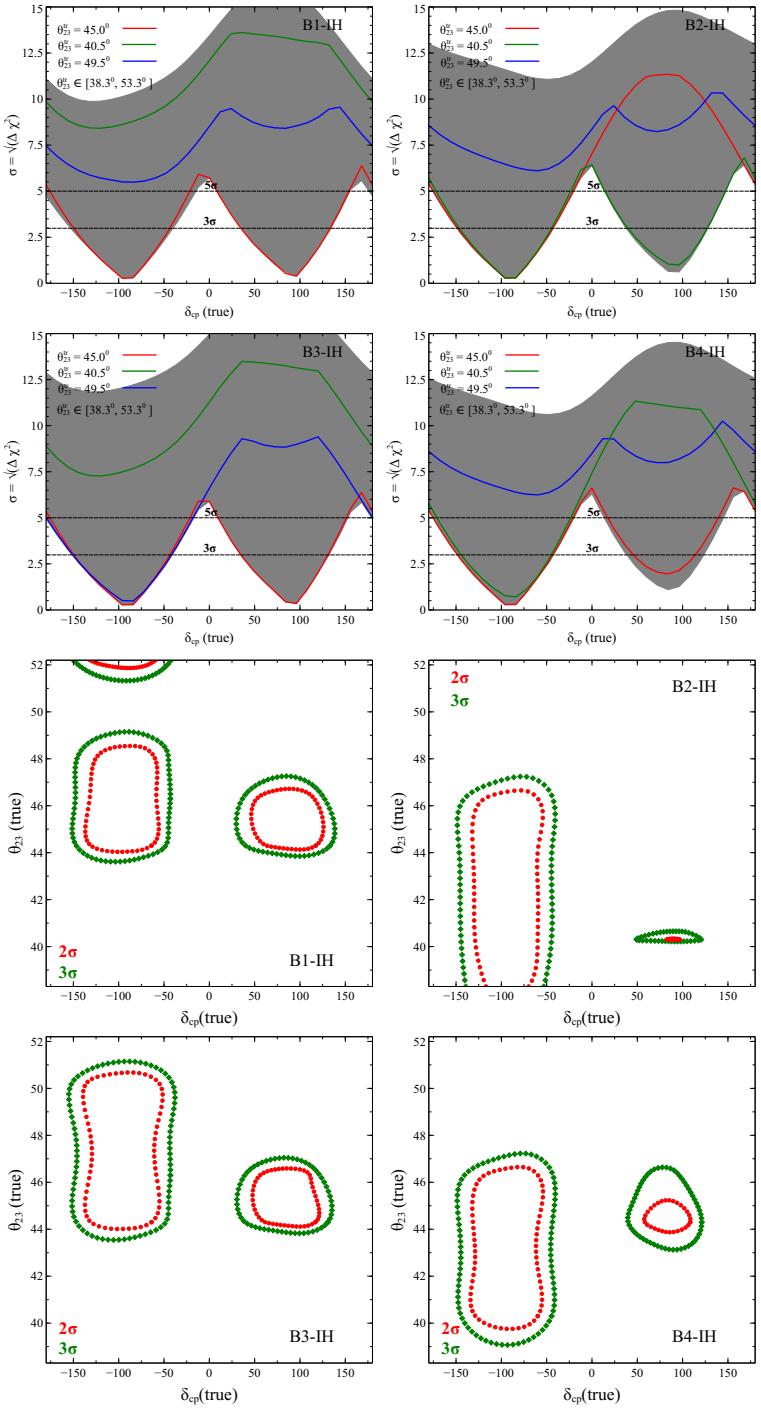

FIG. 8. The sensitivity of different two-zero textures at DUNE assuming IH as the true hierarchy. In the upper panel, the grey band represents the full variation of θ_{23} in its 3σ allowed range. Green, blue and the red plots corresponds to three different choice of θ_{23} i.e. green plot is for the best fit value of θ_{23} in the LO while the blue plot is for θ_{23} in the HO. The red plot is for maximal θ_{23}. In the contour plot, green (red) dotted line represents the 3σ (2σ) contour at 1 d.o.f..

observations can be made from these two panels:

- **B1-IH:** This texture can be excluded for both the octant at 5σ C.L. for all true $\delta_{\rm CP}$. For maximal θ_{23}, B1 is allowed at 5σ C.L. for all true $\delta_{\rm CP}$ except a small fraction around 0^0 and $\delta_{\rm CP} > 150^0$. On the other hand, at 3σ C.L., $\delta_{\rm CP}$ in the range $30^0 < \delta_{\rm CP} < 137^0$ is allowed in the upper half plane (UHP, from 0 to π) while $-150^0 < \delta_{\rm CP} < -37^0$ gives the allowed values of $\delta_{\rm CP}$ in the lower half plane (LHP, from -π to 0).

- **B2-IH:** If LO is the true octant then this texture can not be excluded for most of the true $\delta_{\rm CP}$ at 5σ. Only a small fraction around $\delta_{\rm CP} = 0^0$ and $\delta_{\rm CP} > 150^0$ is excluded at DUNE at 5σ. But for the true HO, B2 can be excluded at 5σ for all true $\delta_{\rm CP}$. If θ_{23} is maximal, then B2 is excluded for all $\delta_{\rm CP}$ in the UHP at 5σ. The allowed fraction of $\delta_{\rm CP}$ lies in between -150^0 and -37^0 at 3σ for $\theta_{23} = 45^0$.

- **B3-IH:** B3 is excluded at DUNE for true LO as well as the HO (for all true $\delta_{\rm CP}$ in the UHP) at 5σ if IH is true hierarchy. For true HO, this texture is allowed only for $-150^0 < \delta_{\rm CP} < -37^0$ at 3σ. Like B1, for maximal θ_{23}, almost all true $\delta_{\rm CP}$ is allowed at 5σ except $\delta_{\rm CP} > 150^0$ and some fraction around 0^0.

- **B4-IH:** Here in this case, B4 is excluded for true HO irrespective of true $\delta_{\rm CP}$. B3 can also be ruled out at 5σ C.L. for all true $\delta_{\rm CP}$ in the UHP and LO is the true octant. In case of maximal θ_{23}, 5σ (3σ) allowed values of $\delta_{\rm CP}$ lie in the range $-175^0 < \delta_{\rm CP} < -25^0$ ($-150^0 < \delta_{\rm CP} < -35^0$) and $15^0 < \delta_{\rm CP} < 137^0$ ($45^0 < \delta_{\rm CP} < 115^0$).

- From the contour plots, we observe that at 3σ C.L., all these four textures in IH mode prefer $\delta_{\rm CP}$ in the range from -150^0 to 50 in the LHP. For these allowed $\delta_{\rm CP}$, B1 can give more precise measurement of θ_{23}. Similarly if $\delta_{\rm CP}$ lies in the UHP, then B2 gives the most precise measurement of θ_{23}.

The results of this analyses are summarized in TABLE IV and TABLE V in terms of θ_{23} and $\delta_{\rm CP}$ allowed regions for different textures.

VI. CONCLUSIONS

To conclude, in this work, we performed a phenomenological study on two-zero and one-zero textures from DUNE prospective. We have studied the sensitivity of DUNE to test the

	NH	NH	IH	IH
Textures	δ_{CP} allowed (3σ)	θ_{23} allowed (3σ)	δ_{CP} allowed (3σ)	θ_{23} allowed (3σ)
G2	$-140^0 < \delta_{CP} < 140^0$	all	$-150^0 < \delta_{CP} < 130^0$	all
G3	$-145^0 < \delta_{CP} < 140^0$	all	$-150^0 < \delta_{CP} < 130^0$	all
G4	$-145^0 < \delta_{CP} < 125^0$	$\theta_{23} < 48^0$	$-150^0 < \delta_{CP} < 125^0$	all
G5	$-140^0 < \delta_{CP} < 125^0$	all	$-150^0 < \delta_{CP} < 125^0$	all
G6	$-140^0 < \delta_{CP} < 137^0$	$\theta_{23} > 43.5^0$	$-150^0 < \delta_{CP} < 125^0$	all

TABLE IV. The 3σ allowed regions (approximated) in $\theta_{23} - \delta_{CP}$ true parameter space for one-zero textures in both the hierarchies. The true values of θ_{23} is varied $\in [38^0, 53^0]$ while δ_{CP} is varied $\in [-\pi, \pi]$.

	NH	NH	IH	IH
Textures	δ_{CP} allowed (3σ)	θ_{23} allowed (3σ)	δ_{CP} allowed (3σ)	θ_{23} allowed (3σ)
B1	-	-	$-150^0 < \delta_{CP} < -40^0$	$43.8^0 < \theta_{23} < 49.2^0$, $\theta_{23} > 51.5^0$
	-	-	$30^0 < \delta_{CP} < 137^0$	$45.9^0 < \theta_{23} < 47.2^0$
B2	$-150^0 < \delta_{CP} < -37^0$	$\theta_{23} > 43.8^0$	$-150^0 < \delta_{CP} < -40^0$	$\theta_{23} < 47.2^0$
	$25^0 < \delta_{CP} < 150^0$	$\theta_{23} > 44^0$	$45^0 < \delta_{CP} < 120^0$	$40.2^0 < \theta_{23} < 40.6^0$
B3	$-150^0 < \delta_{CP} < -37^0$	$\theta_{23} < 47.5^0$	$-160^0 < \delta_{CP} < -37^0$	$43.5^0 < \delta_{CP} < 51.2^0$
	$37^0 < \delta_{CP} < 137^0$	$\theta_{23} < 47.2^0$	$30^0 < \delta_{CP} < 137^0$	$45.9^0 < \delta_{CP} < 47^0$
B4	$-150^0 < \delta_{CP} < -30^0$	$\theta_{23} > 48^0$	$-150^0 < \delta_{CP} < -137^0$	$39^0 < \delta_{CP} < 47^0$
	$37^0 < \delta_{CP} < 137^0$	$\theta_{23} > 49.8^0$	$37^0 < \delta_{CP} < 125^0$	$43^0 < \delta_{CP} < 47^0$

TABLE V. The 3σ allowed regions in $\theta_{23} - \delta_{CP}$ true parameter space for two-zero textures in both the hierarchies. The true values of θ_{23} is varied $\in [38^0, 53^0]$ while δ_{CP} is varied $\in [-\pi, \pi]$.

values of θ_{23} and δ_{CP} predicted by various texture zero mass matrices. We can draw the following conclusions from this study:

- In fig.5, we find that for the three specific values of θ_{23}, none of these textures can be excluded at DUNE at 5σ for all δ_{CP}. G2 and G3 are allowed for all θ_{23} at 3σ when δ_{CP} is in the range from -150^0 to 137^0. G5 also show some similar behaviour. G4 and

G5 can be excluded at 5σ (and hence at 3σ) for some combination of θ_{23} and $\delta_{\rm CP}$ and from the contour plots it is observed that for any θ_{23} from 48^0 to 53^0, G4 is completely excluded at DUNE for all $\delta_{\rm CP}$ at 3σ. On the other hand, for any θ_{23} in the LO from 38^0 to 43^0, G6 is completely excluded for all $\delta_{\rm CP}$ at 3σ. Hence G4 and G6 can give more precise measurements compared to G2, G3 and G6.

- We observe from fig.6 that all the one-zero textures in IH mode are allowed for most of the $\delta_{\rm CP}$ at 5σ for any values of θ_{23} (except $\delta_{\rm CP} = \pm\pi$). G2 has a small exclusion region near $\delta_{\rm CP} = 0^0$ for some θ_{23}. Since, for a large portion of the $\theta_{23} - \delta_{\rm CP}$ true parameter space these textures are allowed at 3σ in IH mode, they are less predictive compared to two-zero texture.

- In fig.7, we observe that for maximal θ_{23} as well as for true HO (which corresponds to $\theta_{23} = 47.7^0$), B2 behaves identically and it is not possible to rule out at 5σ for any $\delta_{\rm CP}$ except the CP conserving values. If the LO is the true octant and $\theta_{23} = 42.3^0$, then DUNE can rule out B2 and B4 at 5σ C.L. for any true $\delta_{\rm CP}$. For maximal θ_{23}, B4 is excluded at 5σ while for true HO it is ruled out completely at 3σ. So for all the three choices of θ_{23} in the present scenario, DUNE can exclude B4 at 3σ C.L.. As seen from the contour plot corresponding to B4, the allowed true $\theta_{23} - \delta_{\rm CP}$ parameter space is very much constraint compared to any other textures. For any θ_{23} from 38^0 to 48^0, B4 is completely excluded for all *dcp* at 3σ. Hence it is the most predictive texture which allow some combinations of θ_{23} and $\delta_{\rm CP}$ in the HO. On the other hand, B3 is not possible to exclude completely at 3σ for the three specific values of θ_{23}.

- In fig.8, we have studied the two-zero textures in IH mode. We conclude that at DUNE we can rule out B1 and B3 at 5σ C.L. for all $\delta_{\rm CP}$ when the true θ_{23} is in the LO. Similarly, DUNE can exclude B1, B2 and B4 at 5σ for θ_{23} in the HO for all $\delta_{\rm CP}$. Maximal θ_{23} is allowed in all the cases. Only in B2, we can exclude maximal θ_{23} at 5σ for all $\delta_{\rm CP}$ in the UHP. From the contour plots, we can conclude that the allowed parameter space is much smaller than one-zero textures. Hence, these are much predictive textures in $\theta_{23} - \delta_{\rm CP}$ parameter space.

- From the analyses, we have observed that the CP conserving scenarios are excluded at 5σ C.L. in all forms of two-zero textures irrespective of hierarchy and θ_{23}. But

in one-zero textures, only $\delta_{\rm CP} = \pm\pi$ is excluded at 3σ C.L. for all θ_{23} in both the hierarchies.

Since the texture zero mass matrices can be generated by different flavour symmetry models considered in several earlier works [43–52], possible discrimination of different texture zeros at DUNE studied in this work could also disfavour certain flavour symmetry models leading to some particular textures. Although the new physics sector is not directly affecting the neutrino oscillation probabilities analytically, its presence is indirectly tested by probing the specific neutrino parameters it predicts through a particular texture zero mass matrix. This study can also be extended to other texture zero models like the ones with non-diagonal charged lepton mass matrix, the ones with additional light sterile neutrinos. We are working on these possibilities which will be presented in an upcoming work [80].

ACKNOWLEDGMENTS

We acknowledge the use of HRI cluster facility to carry out the computations. DD thanks Prof. Raj Gandhi for his support as well as discussions regarding DUNE. He acknowledges the support from Gauhati University and the DAE Neutrino project at HRI to visit Gauhati University and IIT, Guwahati. He also thanks Suprabh Prakash for some useful discussions during his HRI visit.

Appendix A: Light neutrino mass matrix elements

$$M_{ee} = c_{12}^2 c_{13}^2 m_1 + c_{13}^2 s_{12}^2 m_2 e^{i2\alpha} + s_{13}^2 m_3 e^{i2\beta} \tag{A1}$$

$$M_{e\mu} = M_{\mu e} = c_{13}\Big(s_{13}s_{23}m_3 e^{i(\delta_{\rm CP}+2\beta)} - c_{12}m_1(c_{23}s_{12} + c_{12}s_{13}s_{23}e^{i\delta_{\rm CP}}) + s_{12}m_2 e^{i2\alpha}(c_{12}c_{23} - s_{12}s_{13}s_{23}e^{i\delta_{\rm CP}})\Big) \tag{A2}$$

$$M_{e\tau} = M_{\tau e} = c_{13}\Big(c_{23}s_{13}m_3 e^{i(\delta_{\rm CP}+2\beta)} - s_{12}m_2 e^{i2\alpha}(c_{23}s_{12}s_{13}e^{i\delta_{\rm CP}} + c_{12}s_{23}) + c_{12}m_1(-c_{12}c_{23}s_{13}e^{i\delta_{\rm CP}} + s_{12}s_{23})\Big) \tag{A3}$$

$$M_{\mu\mu} = c_{13}^2 s_{23}^2 m_3 e^{i2(\delta_{\rm CP}+\beta)} + m_1(c_{23}s_{12} + c_{12}s_{13}s_{23}e^{i\delta_{\rm CP}})^2 + m_2 e^{i2\alpha}(c_{12}c_{23} - s_{12}s_{13}s_{23}e^{i\delta_{\rm CP}})^2 \tag{A4}$$

$$M_{\mu\tau} = M_{\tau\mu} = c_{13}^2 c_{23} s_{23} m_3 e^{i2(\delta_{\rm CP}+\beta)} + m_1 (c_{12} c_{23} s_{13} e^{i\delta_{\rm CP}} - s_{12} s_{23})(c_{23} s_{12} + c_{12} s_{13} s_{23} e^{i\delta_{\rm CP}}) - m_2 e^{i2\alpha} (c_{23} s_{12} s_{13} e^{i\delta_{\rm CP}} + c_{12} s_{23})(c_{12} c_{23} - s_{12} s_{13} s_{23} e^{i\delta_{\rm CP}}) \quad \text{(A5)}$$

$$M_{\tau\tau} = c_{13}^2 c_{23}^2 m_3 e^{i2(\delta_{\rm CP}+\beta)} + m_2 e^{i2\alpha} (c_{23} s_{12} s_{13} e^{i\delta_{\rm CP}} + c_{12} s_{23})^2 + m_1 (c_{12} c_{23} s_{13} e^{i\delta_{\rm CP}} - s_{12} s_{23})^2 \quad \text{(A6)}$$

---

[1] S. Fukuda et al. (Super-Kamiokande), Phys. Rev. Lett. **86**, 5656 (2001), hep-ex/0103033; Q. R. Ahmad et al. (SNO), Phys. Rev. Lett. **89**, 011301 (2002), nucl-ex/0204008; Phys. Rev. Lett. **89**, 011302 (2002), nucl-ex/0204009; J. N. Bahcall and C. Pena-Garay, New J. Phys. **6**, 63 (2004), hep-ph/0404061; K. Nakamura et al., J. Phys. **G37**, 075021 (2010).

[2] S. Abe et al. (KamLAND Collaboration), Phys.Rev.Lett. **100**, 221803 (2008).

[3] K. Abe et al. [T2K Collaboration], Phys. Rev. Lett. **107**, 041801 (2011).

[4] Y. Abe et al., Phys. Rev. Lett. **108**, 131801 (2012).

[5] F. P. An et al. [DAYA-BAY Collaboration], Phys. Rev. Lett. **108**, 171803 (2012).

[6] J. K. Ahn et al. [RENO Collaboration], Phys. Rev. Lett. **108**, 191802 (2012).

[7] P. Adamson et al. [MINOS Collaboratio], Phys.Rev.Lett. **110**, 171801 (2013).

[8] M. C. Gonzalez-Garcia, M. Maltoni and T. Schwetz, JHEP **1411**, 052 (2014).

[9] D. V. Forero, M. Tortola and J. W. F. Valle, Phys. Rev. **D90**, 093006 (2014

[10] P. Huber, M. Lindner, and W. Winter, Comput.Phys.Commun. **167**, 195 (2005), hep-ph/0407333.

[11] P. Huber, J. Kopp, M. Lindner, M. Rolinec, and W. Winter, Comput. Phys. Commun. **177**, 432 (2007), hep-ph/0701187.).

[12] P. A.

[13] R. Ade *et al.* [Planck Collaboration], arXiv:1502.01589.

[14] A. Gando et. al., [KamLAND-Zen Collaboration], Phys. Rev. Lett. **110**, 062502 (2013).

[15] M. Agostini et. al., [GERDA Collaboration], Phys. Rev. Lett. **111**, 122503 (2013).

[16] A. Gando et. al., [KamLAND-Zen Collaboration], arXiv:1605.02889.

[17] K. Abe et al., [T2K Collaboration], Phys. Rev. **D91**, 072010 (2015).

[18] K. Abe et al. [T2K Collaboration], Phys.Rev.Lett.112, 181801 (2014),1403.1532.

[19] P. Adamson et al. [MINOS Collaboration], Phys.Rev.Lett. (2014),1403.0867.

[20] A. Himmel (Collaboration for the Super-Kamiokande) (2013),1310.6677.

[21] F. Capozzi, G. Fogli, E. Lisi, A. Marrone, D. Montanino, et al. (2013), 1312.2878.

[22] P. Vahle (2016), talk given at the Neutrino 2016 Conference, July 4-9, 2016, London, United Kingdom, http://neutrino2016.iopconfs.org/home.

[23] Fundamental Physics at the Intensity Frontier (2012), 1205.2671, URL https://inspirehep.net/record/1114323/files/arXiv:1205.2671.pdf.

[24] C. Adams et al. (LBNE) (2013), 1307.7335, URL http://www.osti.gov/scitech/biblio/1128102.

[25] D. Ayres et al. (NOÎ¡A Collaboration) (2004), hep-ex/0503053.

[26] R. Patterson, Talk given at the Neutrino 2012 Conference, June 3-9, 2012, Kyoto, Japan, URL: http://neu2012.kek.jp/.

[27] S. K. Agarwalla, S. Prakash, S. Uma Sankar, JHEP**03** (2014) 087, 1304.3251.

[28] V. Barger, A. Bhattacharya, A. Chatterjee, R. Gandhi, D. Marfatia, M. Masud, Phys. Rev. D 89, 011302 (2014), 1307.2519.

[29] N. Nath, M. Ghosh, S. Goswami, (2015), 1511.07496.

[30] K. Bora, D. Dutta, P. Ghoshal, Mod.Phys.Lett.A 30, 1550066 (2015), 1405.7482.

[31] K. Bora, D. Dutta, J. of Physics, Conf. series (IOP UK), vol 481, p 012019, 2014, 1209.1870.

[32] G. L. Fogli and E. Lisi, Phys. Rev.D54, 3667 (1996),[hep-ph/9604415].

[33] K. Hiraideet al., Phys.Rev.D73, 093008 (2006), [hep-ph/0601258].

[34] R. Gandhi, P. Ghoshal, S. Goswami, P. Mehta, S. Uma Sankar, Phys.Rev. D73 (2006) 053001, hep-ph/0411252.

[35] T. Lee, Phys.Rev. **D8**, 1226 (1973).

[36] T. Lee, Phys.Rept. 9, 143 (1974).

[37] V. Barger, A. Bhattacharya, A. Chatterjee, R. Gandhi, D. Marfatia, M. Masud, J. Mod. Phys. A 31, 1650020 (2016),1405.1054.

[38] S. Prakash, S. K. Raut, S. Uma Sankar, Phys.Rev. D86 (2012) 033012, 1201.6485.

[39] S. Kumar Agarwalla, S. Prakash, S. Uma Sankar, JHEP 1403 (2014) 087, 1304.3251.

[40] D.Dutta, K. Bora, Mod.Phys.Lett.A 30, 1550017 (2015), 1409.8248.

[41] K. Bora, G. Ghosh, D. Dutta, Adv.High Energy Phys. 2016 (2016) 9496758, 1606.00554.

[42] P. O. Ludl and W. Grimus, JHEP **1407**, 090 (2014).

[43] M. Berger and K. Siyeon, Phys. Rev. **D64**, 053006 (2001).

[44] C. I. Low, Phys. Rev. **D70**, 073013 (2004).

[45] C. I. Low, Phys. Rev. **D71**, 073007 (2005).

[46] W. Grimus, A. S. Joshipura, L. Lavoura and M. Tanimoto, Eur. Phys. J. **C36**, 227 (2004).

[47] Z. -z. Xing and S. Zhou, Phys. Lett. **B679**, 249 (2009).

[48] S. Dev, S. Gupta and R. R. Gautam, Phys. Lett. **B701**, 605 (2011).

[49] T. Araki, J. Heeck and J. Kubo, JHEP **1207**, 083 (2012).

[50] R. G. Felipe and H. Serodio, Nucl. Phys. **B886**, 75 (2014).

[51] A. Dighe and N. Sahu, arXiv:0812.0695.

[52] W. Grimus and L. Lavoura, J. Phys. **G31**, 693 (2005).

[53] Z. -z. Xing, Phys. Rev. **D69**, 013006 (2004).

[54] E. Lashin and N. Chamoun, Phys. Rev. **D85**, 113011 (2012).

[55] K. Deepthi, S. Gollu and R. Mohanta, Eur. Phys. J. **C72**, 1888 (2012).

[56] R. R. Gautam, M. Singh and M. Gupta, Phys. Rev. **D92**, 013006 (2015).

[57] L. M. Cebola, D. E. Costa and R. G. Felipe, Phys. Rev. **D92**, 025005 (2015).

[58] P. H. Frampton, S. L. Glashow and D. Marfatia, Phys. Lett. **B536**, 79 (2002).

[59] Z. -z. Xing, Phys. Lett. **B530**, 159 (2002).

[60] Z. -z. Xing, Phys. Lett. **B539**, 85 (2002).

[61] A. Kageyama, S. Kaneko, N. Shimoyana and M. Tanimoto, Phys. Lett. **B538**, 96 (2002).

[62] S. Dev, S. Kumar, S. Verma and S. Gupta, Phys. Rev. **D76**, 013002 (2007).

[63] P. Ludle, S. Morisi and E. Peinado, Nucl. Phys. **B857**, 411 (2012).

[64] S. Kumar, Phys. Rev. **D84**, 077301 (2011).

[65] H. Fritzsch, Z. -z. Xing and S. Zhou, JHEP **1109**, 083 (2011).

[66] D. Meloni and G. Blankenburg, Nucl. Phys. **B867**, 749 (2013).

[67] D. Meloni, A. Meroni and E. Peinado, Phys. Rev. **D89**, 053009 (2014).

[68] S. Dev, R. R. Gautam, L. Singh and M. Gupta, Phys. Rev. **D90**, 013021 (2014).

[69] S. Dev, L. Singh and D. Raj, Eur. Phys. J. **C75**, 394 (2015).

[70] M. Borah, D. Borah and M. K. Das, Phys. Rev. **D91**, 113008 (2015).

[71] S. Kaneko and M. Tanimoto, Phys. Lett. **B551**, 127 (2003).

[72] S. Kaneko, M. Katsumata and M. Tanimoto, JHEP **0307**, 025 (2003).

[73] S. Dev and S. Verma, Mod. Phys. Lett. **A25**, 2837 (2010).

[74] M. Bando, S. Kaneko, M. Obara and M. Tanimoto, Prog. Theor. Phys. **112**, 533 (2004).

[75] T. P. Nguyen, Mod. Phys. Lett. **A29**, 1450038 (2014).

[76] R. Kalita and D. Borah, Int. J. Mod. Phys. **A31**, 1650008 (2016).

[77] P. Huber, M. Lindner, and W. Winter, Comput.Phys.Commun. **167**, 195 (2005), hep-ph/0407333.

[78] P. Huber, J. Kopp, M. Lindner, M. Rolinec, and W. Winter, Comput. Phys. Commun. **177**, 432 (2007), hep-ph/0701187.

[79] Z.-z. Xing, pp. 442–449 (2004), hep-ph/0406049.

[80] K. Bora, D. Borah and D. Dutta, *In preparation.*